The detection of sub-micron phase defects on multi-phase random logic reticles

C. Spence, J. Nistler, W. Arnold
Advanced Micro Devices

D. Emery, L. Zurbrick, D. Prakash, X. Chang,
S. Khanna, B. Leback, E. Tsujimoto
KLA-Tencor

G. Hughes
DuPont RTC

Abstract

In this paper we present results of an algorithm that has been developed which is sensitive to phase defects of 60° on i-line alternating PSMs. This algorithm consists of microcode and software which can be loaded into existing inspection hardware. The algorithm works in die-to-die inspection mode and uses both transmitted and reflected light images to maximize sensitivity. Isolated phase defects as well as phase defects close to chrome edges were inspected. In addition, the algorithm is able to detect missing and misaligned shifter edges. A programmed phase defect test plate was developed to characterize defect detection sensitivity. Detection of 60° defects smaller than 0.75μm has been demonstrated with this algorithm. Defect sensitivity characterization and actual production plate defect results are shown.

1.0 Introduction

Alternating Phase Shift Mask (PSM) was first described and practiced by Levenson et al in the early eighties[1,2]. There are several factors which have delayed the introduction of Alternating PSMs in wafer mass-production, the chief of which has been the steady improvement in i-line stepper lenses and resist processes which have supported mass production down to the 0.35μm generation using conventional (binary) chrome masks. The difficulties involved in the transition to Deep-UV (DUV) lithography with Chemically Amplified resists caused semiconductor manufacturers to consider PSM as an option to extend the useful life of i-line lithography. For some types of circuits, e.g. memory arrays, repetitive designs lead to obvious and simple Alternating PSM designs[3,4]. For random logic circuits, however, design was much more complicated, nonetheless several design approaches have been proposed (especially for the poly gate layer) which appear promising[5,6,7]. At AMD we have pursued our own design approach, which has been used in the production of microprocessors[8]. To use Alternating PSMs in manufacturing it has been necessary to develop a mask process which has tight control of phase angle and zero printing defects. We have chosen to use a 'Multi-Phase' approach[9] to achieve these goals as outlined in the next section.

2.0 Multi-Phase PSMs and Sensitivity of Linewidth to 60° defects

One of the major problems in using alternating PSMs is obtaining masks with no printing defects. If a single quartz etch is performed then 180° phase defects will be created. 180° phase defects are likely to print, and, at present, repair of such defects is very difficult. In the Multi-Phase PSM[8], however, three partial etches of 60° into the quartz substrate are performed. In the case of dark-field masks, the same phase pattern is written three times and the chrome opening defines the etched regions. In the case of light field masks, three different patterns are written in order to produce stepped patterns where phase shift patterns are etched into quartz (Figure 1). By performing three phase etches we perform a 'voting' procedure and so the worst phase defects will have phase shifts of only 60°. This process has the following benefits: firstly, the iterative etch process allows accurate targeting of the desired (180°) phase angle, secondly, the weak modulation of the 60° phase edges (which is even weaker at the reticle inspection wavelength of 488nm) allows us to perform die-to-database inspection of the final reticle with only a slight reduction in sensitivity to chrome defects, and finally, when in focus, the 60° defects have little impact on the final resist pattern. The combination of

0277-786X/98/$10.00

die-to database transmitted light inspection and wafer print evaluations of the final reticles have allowed us to verify the integrity of multiphase reticles and permit their use in production.

The impact of the 60° defects is principally to reduce the process window if we go out of focus. Figure 2 depicts aerial image simulations showing the impact on linewidth of defects of varying sizes placed close to a line (2a) and in-between two lines (2b). The simulation is for the case of a 0.30μm line on a 1.0μm pitch and the stepper parameters chosen were 0.48 NA, 0.48σ at an i-line exposure wavelength. When in focus we see that the predicted CD variation due to 60° defects is less than ±10% for defect sizes up to 0.30μm (1X), i.e. 1.5μm on the reticle for both defect types. This insensitivity to 60° defects has allowed us to use Alternating PSMs for test masks, without requiring repair, before a robust mask fabrication process was available. When the image is out of focus the presence of phase defects can cause the wafer CD to become out of spec sooner than would have been the case if the defect were absent. It can also be seen that the impact of defects away from the line on CD is much less than for those defects close to the line. Thus 60° phase defects are not completely benign, and so to ensure mask quality without requiring wafer print studies and to advance the capability of the quartz etch process it was decided to develop an inspection algorithm for 60° phase defects. Based on the simulations shown in figure 2 and other similar simulations reflecting the full range of design rules encountered we determined that if the PSM detection algorithm was be able to find all 60° defects greater than 0.75μm less than 10% CD variation due to phase defect would occur.

3.0 Defect Test Mask Design

In order to test the 60° defect inspection algorithm a test mask was designed. The PSM design for an SRAM pattern was used and various programmed defects were introduced. The programmed defects ranged in size (designed) from 0.25μm up to 2.0μm. Figures 3a-d show layout plots of some of the defect types. In addition to particle defects the test plate featured cells which had mis-aligned (in X and Y) shifters and in some cases completely missing shifters. Table 1 contains a summary of all the defect types on the plate. Reference die, with no programmed defects, were also included on the plate to allow die-to-die inspection.

Table 1: Programmed test plate defect description

Row	Defect Description
A	Isolated 60° defect in 0° background (divot)
B	Isolated 120° defect in 180° background (bump)
C	60° defect next to chrome line in 0° background (divot)
D	120° defect next to chrome line in 180° background (bump)
E	60° defect in 120° transition away from chrome
F	180° defect in 120° transition away from chrome
G	60° defect in 120° transition next to chrome
H	180° defect in 120° transition next to chrome
I	X Mis-aligned shifters and missing shifter[+]
J	Y Mis-aligned shifters and missing shifter[+]

[+] - Missing shifter defects were placed in rows I and J in columns 1-3

When writing the phase layers an ALTA 3000 was used to avoid charging problems which can occur when patterning resist on top of quartz with e-beam systems. Three phase layers were written and etched, the plate did not receive an undercut etch. Unfortunately, the ALTA 3000 cannot reliably resolve features below 0.75μm and so we measured the defects on the test plate to find out what was the actual defect size. Because of charging problems we were unable to measure the 60° defects with an SEM and so defect measurements were done using a SiScan 325nm optical confocal microscope. The results are summarized in table 2 for defect types A-D. The measurement algorithm used was outside-to-outside and so probably overestimated the size of the defects on the mask.

Design Size	Defect - A	Defect - B	Defect - C	Defect - D
0.25				
0.375				
0.50		0.255	0.425	0.566
0.625	0.271	0.558	0.643	0.648
0.75	0.768	0.66	0.839	0.837
0.875	0.915	0.835	0.982	0.985
1.00	1.129	1.038	1.126	1.102

4.0 Outline of Inspection Algorithm

The inspection algorithm performs a die-to-die comparison of shifter edges and chrome pattern. Phase shift edges are detected using a simultaneous combination of transmitted and reflected light images. The KLA 301 inspection station hardware (shown schematically in Figure 4) utilizes a scanning laser spot to digitize reticle images[10]. A benefit of this approach is that transmitted and reflected light signals are simultaneously generated which are spatially and temporally aligned. The use of both transmitted and reflected light signals was chosen in order to maximize signal to noise characteristics of the phase shift edge signal. This is particularly important since the phase edges are designed to have minimum modulation (signal) so as not to print in the wafer lithography process.

The inspection algorithm is comprised of 1) an image processing algorithm to detect phase edges, 2) a memory buffer to store phase edge information, 3) an alignment subsystem to align phase edge information between the die being inspected, and 4) a defect detector subsystem which compares phase edge information and generates a defect signal when difference are detected. In addition, a binary detector is incorporated to detect chrome defects in parallel to the phase edge inspection. As a reticle is inspected, the image processing algorithm extracts phase edge information and stores it into the memory buffer. This phase edge information is read from the memory buffer while the next die on the reticle is being scanned. The stored phase edge information is aligned to the phase edge information currently being generated during the scan. This aligned phase edge data is sent to the defect detector which compares the two data streams and generates a defect signal when the data is significantly different from one another. This defect information is then processed and sent to the KLA 301 inspection system user interface for display. Figure 5 illustrate this process: the transmitted and reflected light images of the reference and comparison die (5a and 5b respectively) are processed and phase edges are identified (figure 5c). From comparison of the edge information we can identify any defects present.

5.0 Inspection Results

Based on the analysis described in section 2 the target sensitivity for the algorithm was to detect all 60° defects greater than 0.75μm with a false defect rate of less than 1 per cm^2. Table 3 shows the results obtained with the final algorithm. The percentages are based on 20 runs.

Table 3 Detection rates for different 60° defect types

	0.25	0.375	0.50	0.625	0.75	0.875	1.0	1.25	1.5	2.0
A				100%	100%	100%	100%	100%	100%	100%
B			100%	100%	100%	100%	100%	100%	100%	100%
C			10%	85%	100%	100%	100%	100%	100%	100%
D			100%	100%	100%	100%	100%	100%	100%	100%
E			10%	85%	100%	100%	100%	100%	100%	100%
F				40%	100%	100%	100%	100%	100%	100%
G				25%	70%	100%	100%	100%	100%	100%
H					70%	100%	100%	100%	100%	100%
	missing shifter	**missing shifter**	**missing shifter**	**0.125 misalign**	**0.250 misalign**	**0.375 misalign**	**0.500 misalign**	**0.625 misalign**	**0.750 misalign**	**0.875 misalign**
I	100%	100%	100%		50%	100%	100%	100%	100%	100%
J	100%	100%	100%		10%	70%	65%	100%	100%	100%

The defect specification was easily met for defects A-F. Defects G and H are particularly challenging since they represent defects in transition edges near chrome edges. Since, by definition, these defects do not occur in the most critical locations (which was verified by simulations) we relaxed the defect specification for defects G and H to 0.875μm. It should be noted that the test mask had not received an isotropic undercut etch, which is typically used to match transmissions between etched and unetched openings. After such an etch the printability of 60° defects is further reduced. At the defect sensitivity shown above the false defect rate was less than 1 defect per cm^2.

Sensitivity to shifter misalignment is shown in columns I and J. The specification is that all mis alignments greater than 0.75μm should be detected. Table 3 shows 100 percent detection down to 0.625μm. From table 3 it appears that the sensitivity to X misalignment is greater than to Y misalignment, however, inspection of the layout of defects I and J (Figures 6a and 6b respectively) shows that the patterns used for detecting X and Y misalignment are not equivalent, specifically, the X misalignment causes a greater length of shifter edge to be displaced leading to a greater chance of detecting an X misalignment.

The algorithm has been used to inspect real microprocessor designs. Specifically we have looked at fifth- and sixth-generation x86 microprocessor designs. Typically the reticles for these microprocessors comprise greater than $100cm^2$ written area on the reticle. The die-to-die inspection rate using the PSM algorithm is on the order of 1.25 hours using a 2-channel 301 STARLight system. The false defect rate, when running on production plates, was <1 per cm^2. Figures show some of the defect types that have been found using the algorithm. We see that the real reticles exhibit many of the same defects that were designed on the test reticle, i.e. defects in shifter edges (fig. 7), isolated shifter defects (fig. 8) and missing shifter edges (fig. 9). In addition, some more complex defect types were seen (fig. 10)

6.0 Extension to DUV Multiphase Reticles

The present algorithm operating on a 488 nm wavelength inspection tool is not capable of detecting the very weak signals generated by 60° phase edges on DUV (248 nm) reticles. However, an abbreviated theoretical study was performed in order to determine whether this algorithm could be extended to inspect DUV multiphase reticles. The nature of study was to examine the transmitted light signal generated by a hypothetical inspection tool operating at 365 nm wavelength. This wavelength was chosen based upon the relative phase angles of i-line shifters inspected at 488 nm being similar to that of DUV shifters inspected at 365 nm. See Table 4 below. Reflected light simulation results are not reported here since they are similar to the reported transmitted light simulation results.

Table 4 60° Shifter Phase Angle at Inspection Wavelength

Reticle Type	Inspection Wavelength	
	488 nm	365 nm
i-line	44.8°	60°
DUV	30.5°	40.8°

An aerial image simulation was performed for the existing 488 nm inspection tool (KLA 300 series) and for a hypothetical inspection tool with the same optical parameters except for illumination wavelength. Figure 11 illustrates the mask layout and dimensions used in the simulation. Figure 12 illustrates the transmitted light signal with the 488 nm inspection tool for the i-line reticle and two DUV multiphase reticle types. Figure 13 illustrates the transmitted light signal with the 365 nm inspection tool for the DUV reticles and shows the i-line reticle/488 nm inspection tool signal for reference. For figures 12 and 13, the X scale was adjusted for each curve so as to overlay the shifter edges. This was done so that the signals could be directly compared.

It can be seen from figures 12 and 13 that the phase edge signal increases for the DUV reticle phase edges by decreasing the inspection wavelength. Although not equivalent to the i-line reticle / 488 nm inspection tool signal, the DUV reticle / 365 nm inspection tool signal is adequate for detecting phase edges. These results indicate that it should be possible to extend this algorithm to DUV reticle inspection at shorter inspection wavelength.

7.0 Summary and Conclusions

We have presented details of a new algorithm which allows detection of 60° phase defects on i-line alternating PSMs. The algorithm, which runs on a KLA 300 works in die-to-die mode and uses both transmitted and reflected light signals to maximize the sensitivity of the KLA 300 to these weakly-modulated signals. Detection of 60° defects smaller than 0.75μm, in a variety of locations, has been demonstrated with this algorithm.

Acknowledgments

The authors would like to thank Paul Ackmann and Stuart Brown (AMD Fab 25) for providing manufacturing data, Regina Schmidt (AMD SDC) for performing some defect printability simulations and Peter Rijans (DuPont Photomasks Inc.) for SiScan measurements on the Phase Defect plate.

References

1. M.D Levenson, N Vishwanath and R Simpson. IEEE ED-29, pp. 1828-1836 (1982)
2.M.D. Levenson, D.S. Goodman, S. Lindsey, P.W. Bayer and H.A. Santini. IEEE ED-31, pp. 753-763 (1984)
3.T. Terasawa, N. Hasegawa, T. Kurosaki and T. Tanaka, Proc. SPIE Vol. 1088 pp. 25-33 (1989)
4.S-G Kim, S-G Woo, W-S Han, Y-B Koh and M-Y Lee Proc SPIE vol. 2440 pp 515-523 (1995)
5.G. Galan, F. Galan, P. Schiavone and J.M. Temerson J. Jap. Appl. Phys. 33 pp 6778-6784 (1994)
6.L. Leibmann, T. Newman, R. Ferguson, R. Martino, A. Moless, M. Neisser and T. Weed Proc. SPIE vol. 2197 pp. 612-623 (1994)
7. Y.C. Pati, Y-T Wang, J-W Ling and T Kailath proc SPIE vol. 2197 pp 314-327 (1994)
8.P. Ackmann, S. Brown, J. Nistler and C. Spence, Proc. SPIE vol 3051 pp 146-153 (1997)
9. J. Nistler, G. Hughes, A. Muray and J. Wiley Proc. SPIE vol. 1604, p. 236 (1991)
10. M.Brandemuehl, et al, "Introduction to the KLA 331 Next Generation Reticle Inspection System", BACUS News, Volume 8, Issue 9, Sept. 1992, p1-8

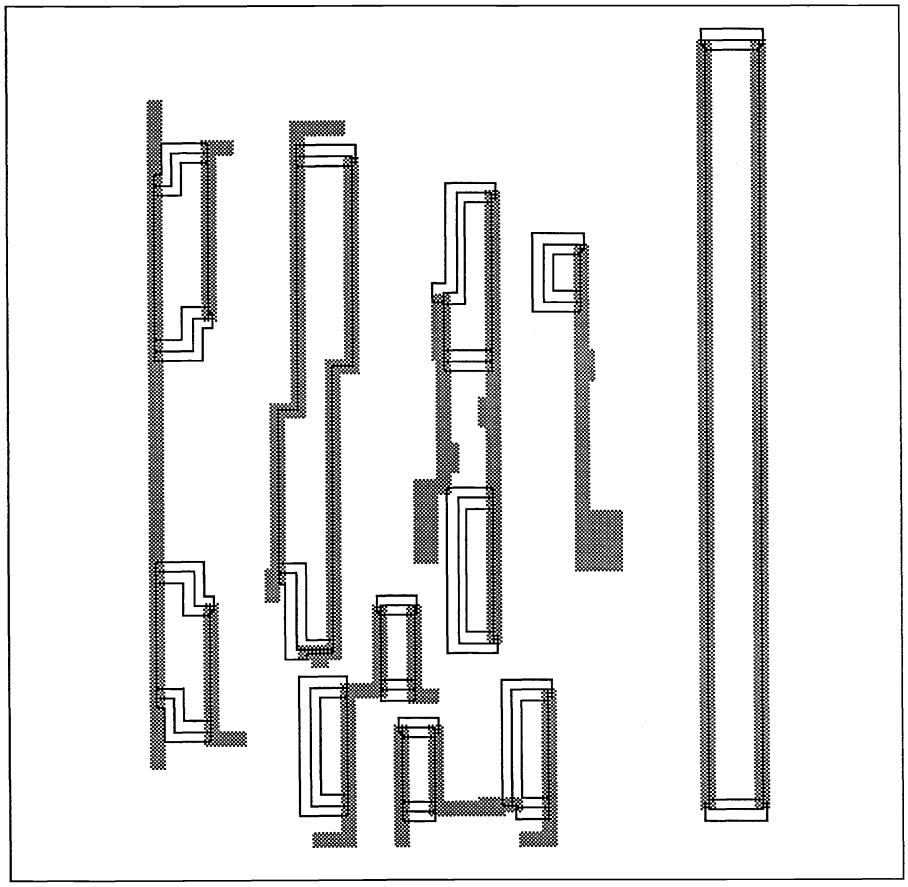

Figure 1 - Clear Field PSM Design

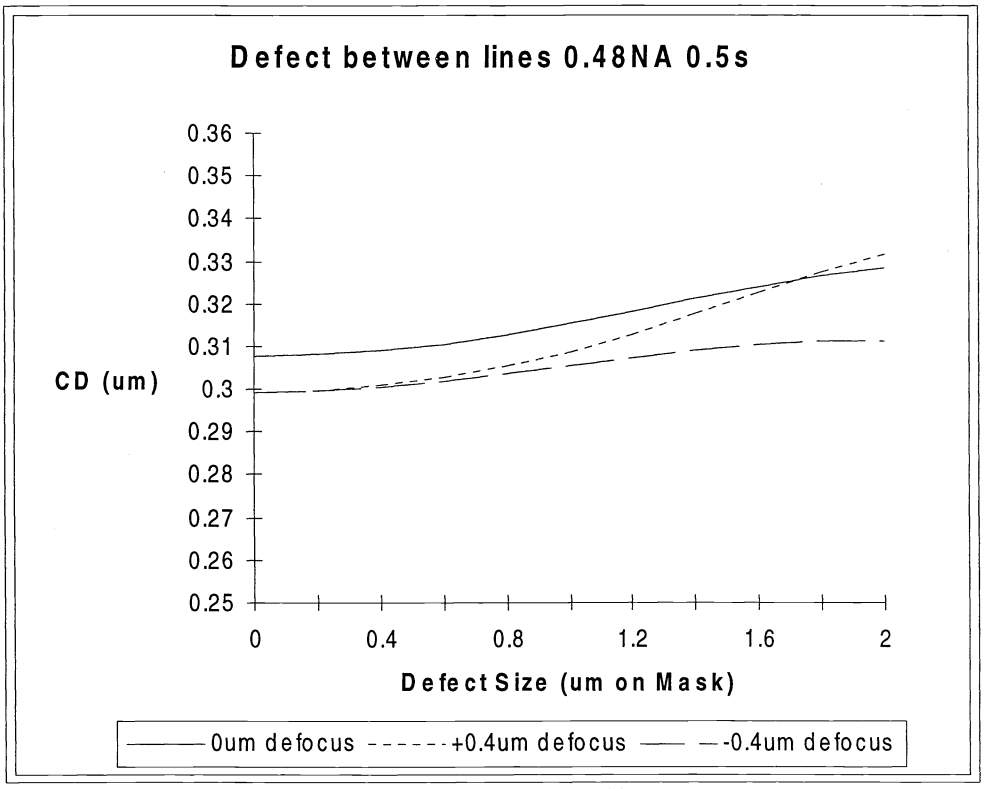

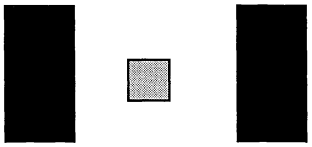

Figure 2A - Simulation Aerial Image: Defect Away From Chrome

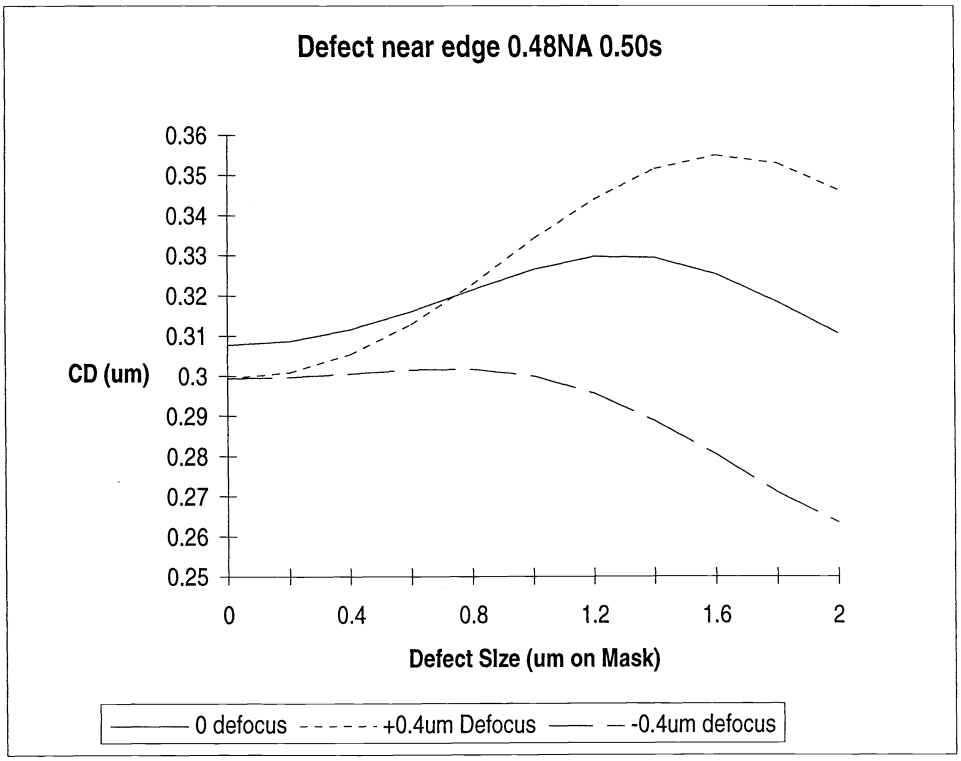

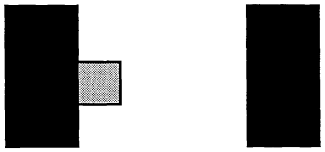

Figure 2B - Simulation Aerial Image: Defect Near Chrome

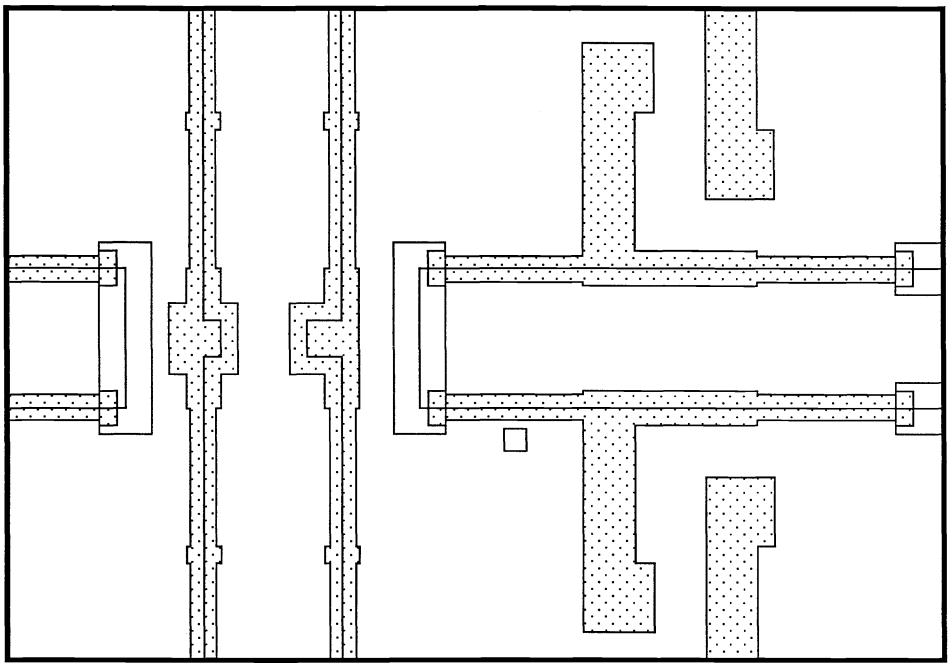

Figure 3A - Defect Type "A"

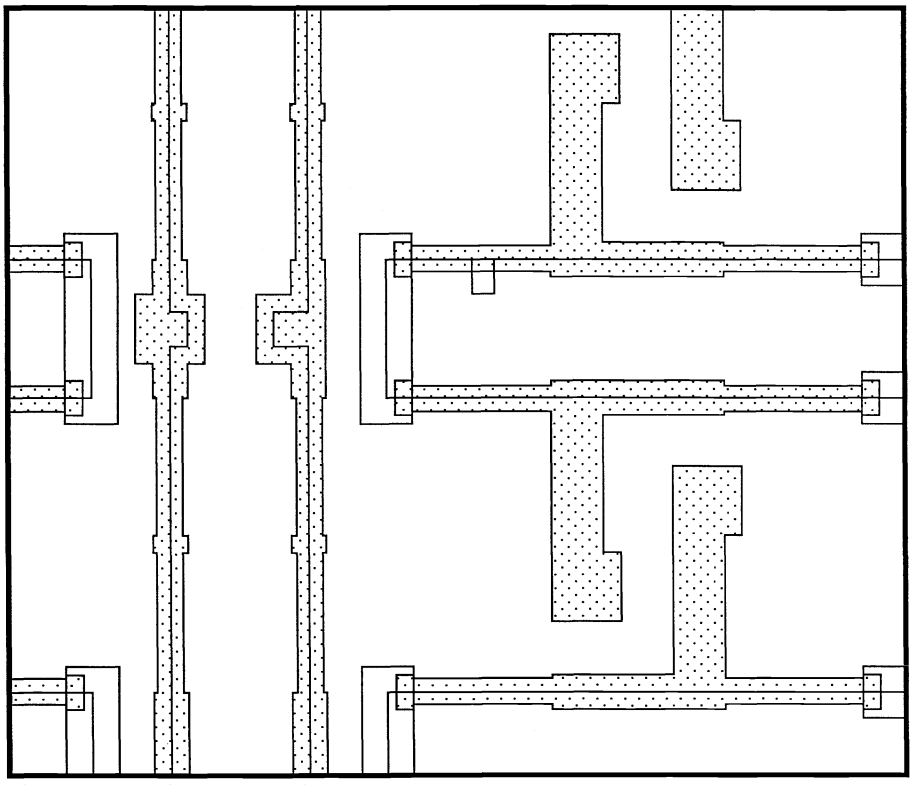

Figure 3B - Defect Type "D"

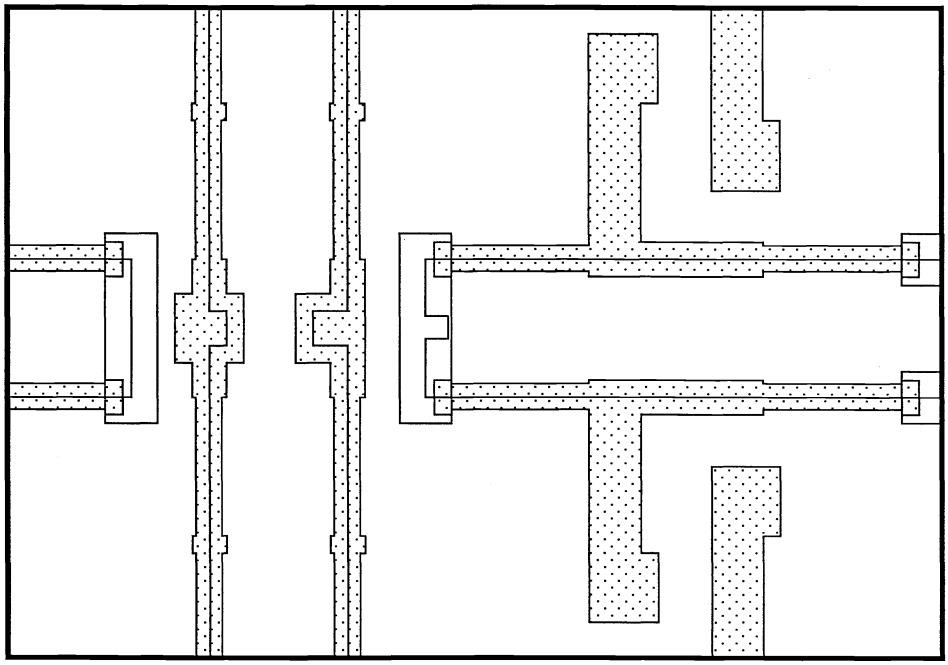

Figure 3C - Defect Type "E"

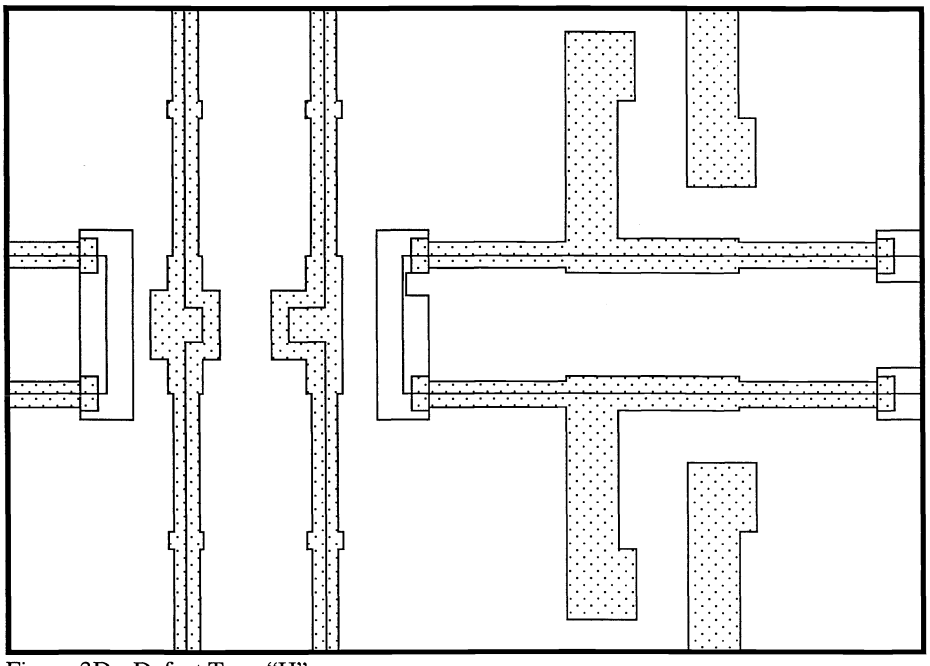

Figure 3D - Defect Type "H"

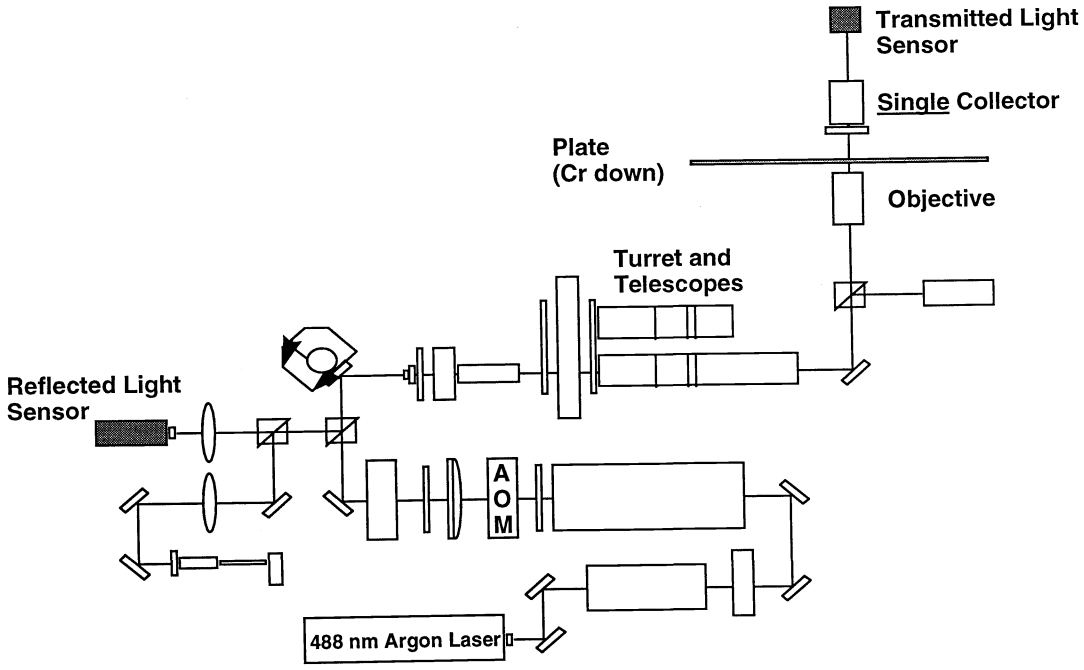

Figure 4 - KLA 351 Optical Layout

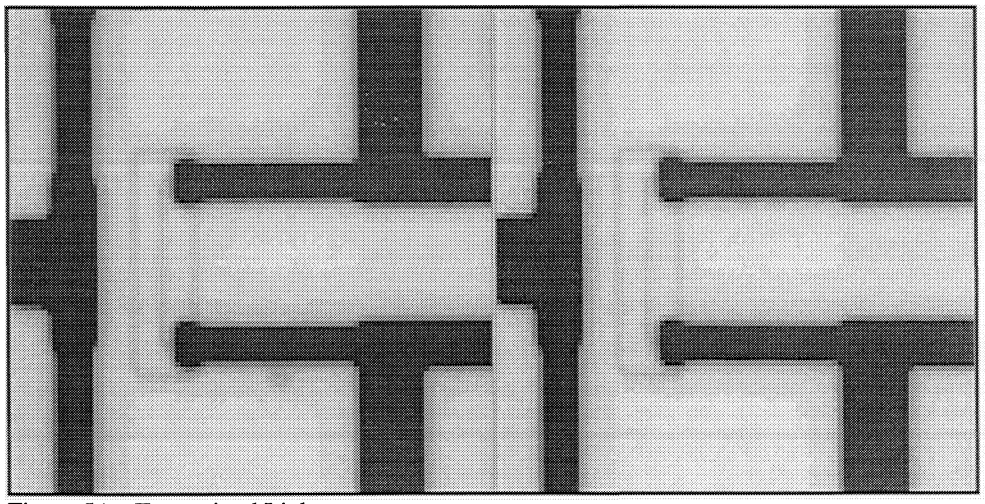

Figure 5A - Transmitted Light

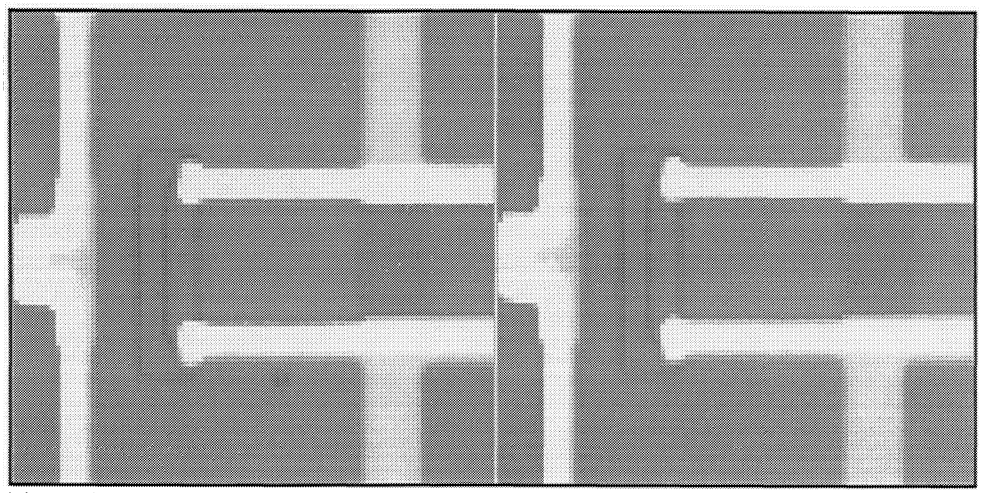

Figure 5B - Reflected Light

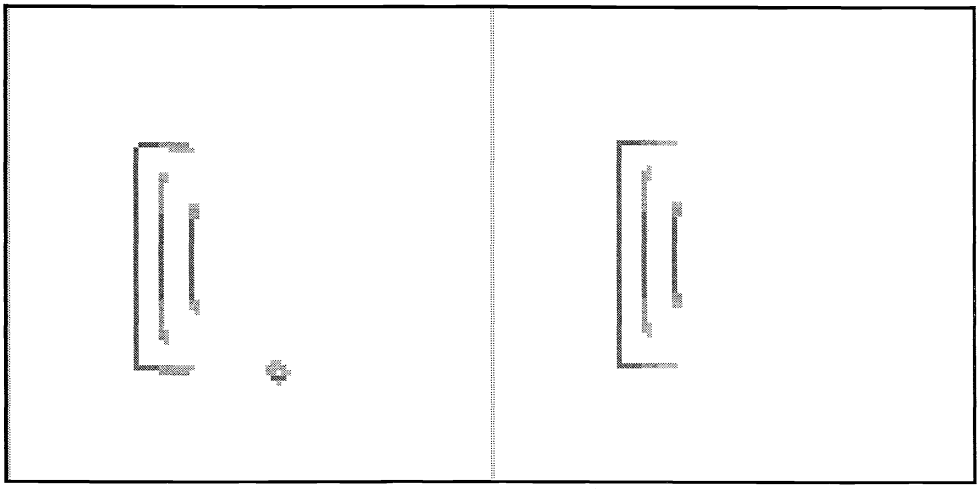

Figure 5C - Shifter Edges

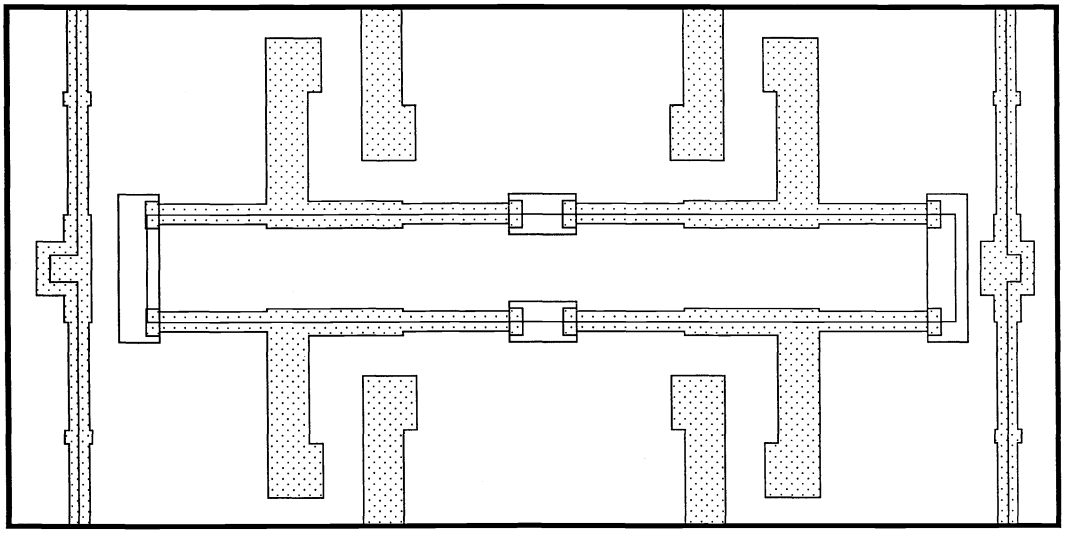

Figure 6A - X Misalign Shifter Defect

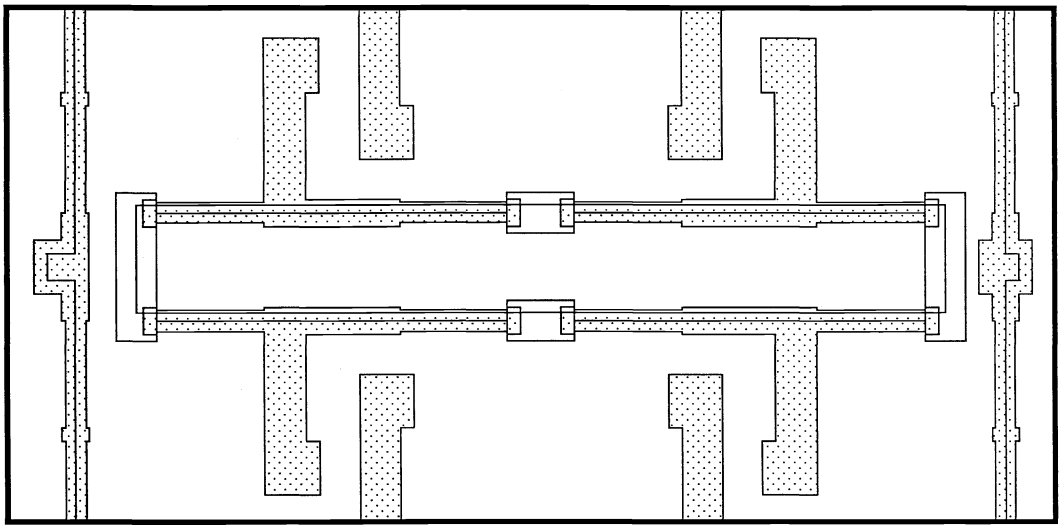

Figure 6B - Y Misalign Shifter Defect

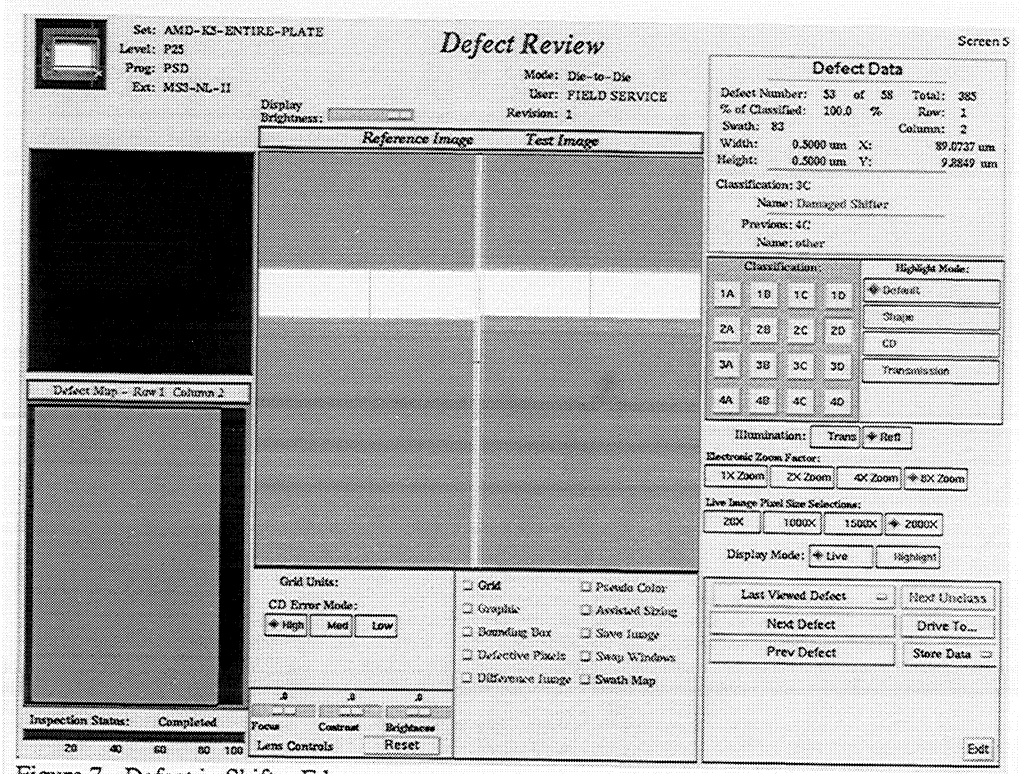

Figure 7 - Defect in Shifter Edge

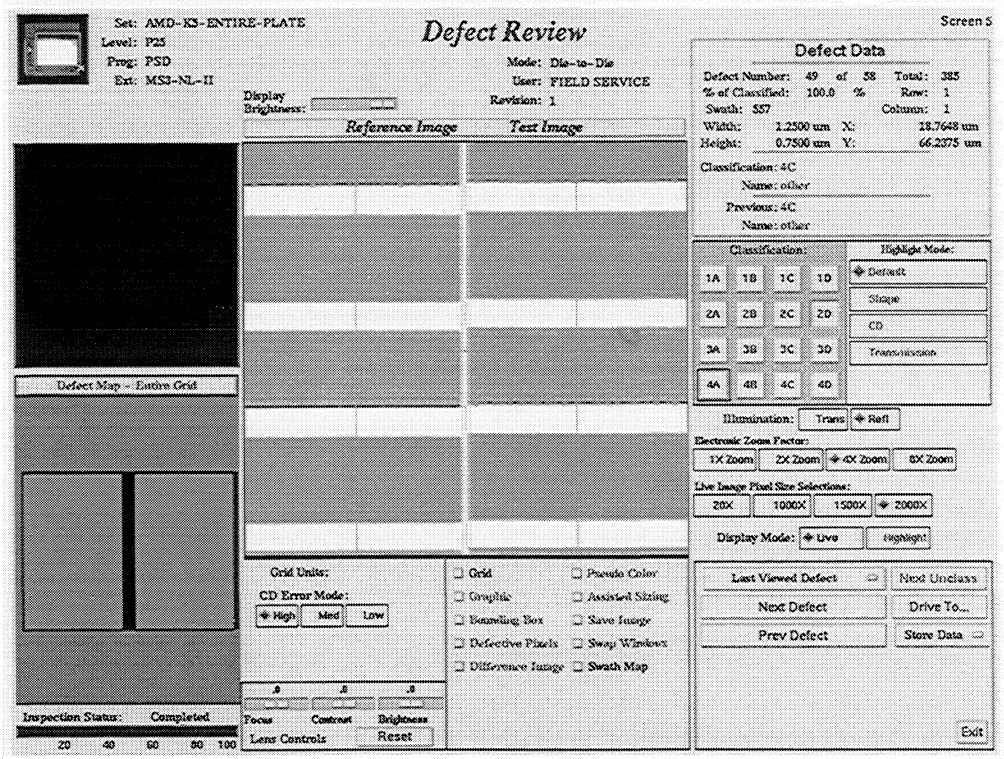

Figure 8 - Isolated Shifter Defect

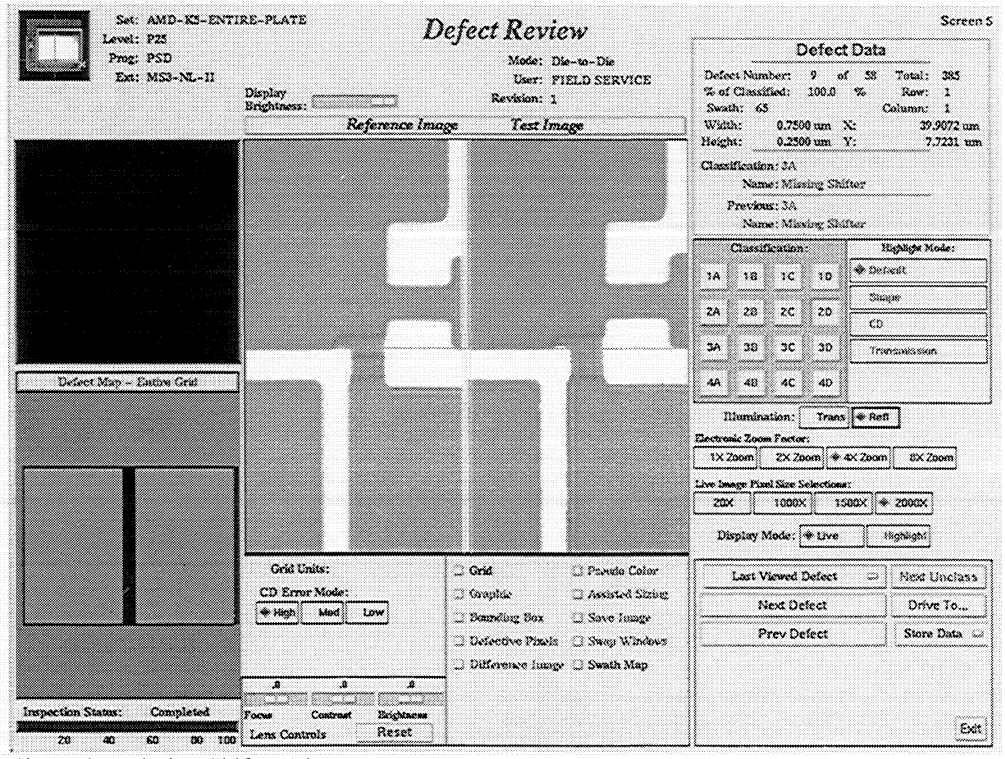

Figure 9 - Missing Shifter Edge

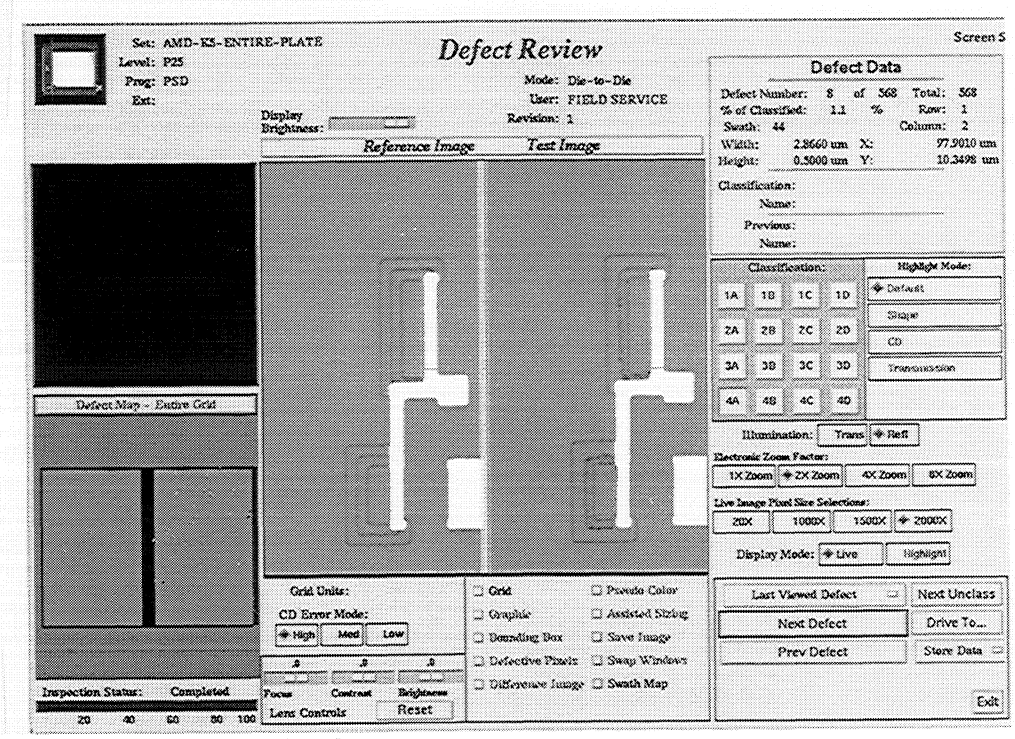

Figure 10 - Complex Defect Type

	i-line 5X	DUV 4X	DUV 5X
Wafer CD	0.4	0.25	0.25
A	2 µm	1 µm	1.25 µm
B	3 µm	1.5 µm	1.88 µm
C	1.5 µm	0.75 µm	0.94 µm
D	1.5 µm	0.75 µm	0.94 µm

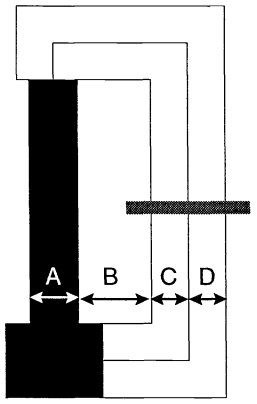

Simulation Results Region

Figure 11 - Aerial Image Simulation Mask Input Parameters

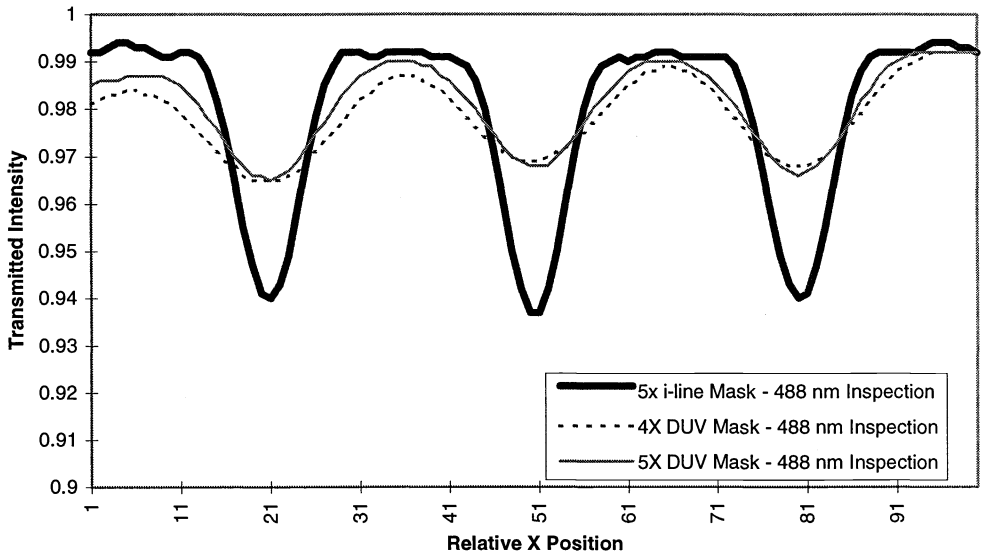

Figure 12 - Transmitted Light Signal Simulation Results for 488 nm Inspection Tool

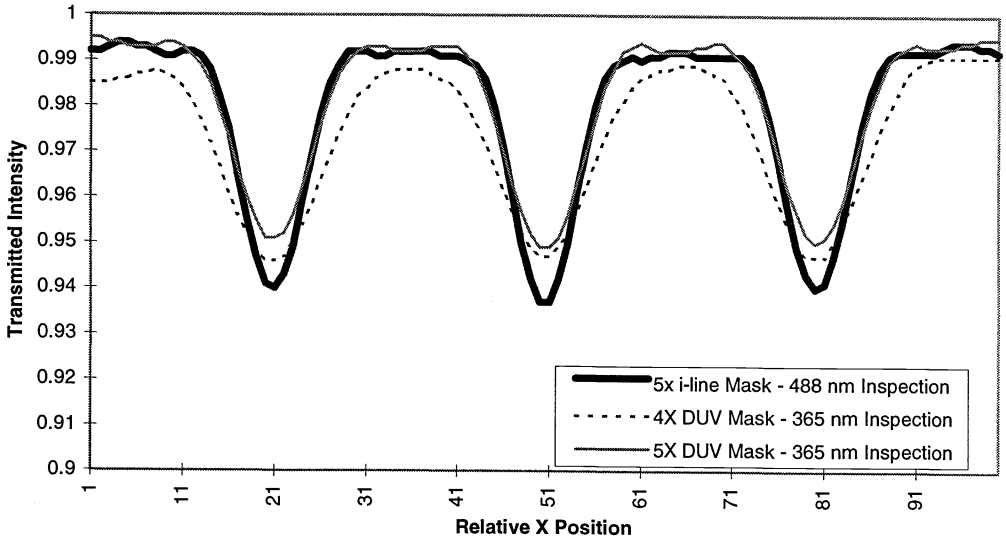

Figure 13 - Transmitted Light Signal Simulation Results for Hypothetical 365 nm Inspection Tool